Toward target-oriented FWI: An exact local wave solver applied to salt boundary inversion

Bram Willemsen, M.I.T, Winston Lewis, Schlumberger and Alison Malcolm, formerly at M.I.T, presently at Memorial University

SUMMARY

Seismic full waveform inversion (FWI) uses the gradient of the objective function for computing model updates. This requires computation of the forward and adjoint wavefields on the current model estimate. Calculating the gradient on the full computational domain is wasteful when it is only required in a limited region of interest, as is the case in 4D seismic and salt boundary estimation, for example. In this paper, a local solver is introduced that accurately computes, up to machine precision, all the wavefield interactions between model updates restricted to a region of interest and inhomogeneities in the background model outside. The local solver therefore generates exactly the same forward and adjoint wavefields in the region of interest that a full domain solver would have generated. In this paper, the exact local gradient at the boundary of a salt body is computed from these exact local wavefields. A level set method uses this gradient to automatically update the local salt boundary estimate.

INTRODUCTION

FWI is a computationally intensive problem. Improvements have been made on many fronts, including the convergence speed of the inverse problem (Métivier et al., 2013), the number of forward solves required (Krebs et al., 2009; Herrmann et al., 2013), and the computational cost of a forward solve (Wang et al., 2011; Zepeda-Núñez and Demanet, 2014). When our primary interest is in a specific section of the model, the problem can be reduced in size with further computational gains as a result. One way of doing this is through seismic redatuming (Berryhill, 1984; Wiggins, 1984) in which a seismic survey is propagated to a virtual survey at the region of interest. This approach introduces artifacts, as is demonstrated by, for instance, Haffinger (2012). Another technique approximates the local wavefield within the region of interest in terms of local model updates (i.e., scatterers). These wavefields can then be used for inversion.

Several authors have investigated the computation of local wavefields with varying levels of approximation for many different types of model configurations. A special configuration is an infinite homogeneous medium with scatterers introduced by perturbing the model in one region of interest (Teng, 2003; Gillman et al., 2013) or multiple disjoint regions (Grote and Sim, 2011). The restriction to infinite homogeneous media prevents applications in seismology. Robertsson and Chapman (2000) approximate the wavefield within a locally perturbed subdomain embedded in an inhomogeneous background medium, but do not include the effect of the perturbed wavefield scattering at inhomogeneities in the background outside of the subdomain and subsequently reentering the subdomain. van Manen et al. (2007) included these reentering waves when they intro-

duced an exact domain truncation method in the time domain that will work for inhomogeneous background models. Using their method, including these reentering waves, comes with a significant cost. The method that is introduced in this paper also generates the wavefield exactly in a locally perturbed subdomain embedded in an inhomogeneous background medium. The approach shares similarities with the work of van Manen et al. (2007), but implements a boundary condition around the subdomain in the frequency domain for computational efficiency. In this paper, the local solver is applied to the problem of automatically updating the shape of a salt body in the velocity model. A level set method (Lewis et al., 2012) parametrizes and updates the shape of the salt body in an implicit way.

LOCAL SOLVER

To introduce the local solver, we group the nodes of the finite difference grid into domains as is illustrated by Figure 1. The full computational domain Ω is the union of all these domains:

$$\Omega = A \cup B \cup \partial C \cup C. \qquad (1)$$

The perturbed model $m(x)$ is defined as:

$$m(x) = m_0(x) + \delta m(x), \qquad (2)$$

where $m_0(x)$ is the background model, which is the initial guess or model in an inversion context. The model is the squared slowness. The model perturbations $\delta m(x)$ are restricted to C (i.e., the yellow nodes in Figure 1), which is the interior of the truncated domain:

$$\mathrm{supp}\,(\delta m) \subset C, \qquad (3)$$

where supp() refers to the support of its argument. We stress that the truncated domain $\partial C \cup C$ can have arbitrary shape and is not limited to a square. We define the scattered field as:

$$u_s(x) = u(x) - u_0(x), \qquad (4)$$

where $u_s(x)$ contains all orders of scattering and $u(x)$ is the wavefield in the perturbed model satisfying

$$-m(x)\omega^2 u(x,\omega) - \Delta_h u(x,\omega) = f(x,\omega), \qquad (5)$$

with Δ_h the discrete Laplacian with node spacing h. In this paper, a second-order accurate stencil is used. The wavefield in the background model u_0 satisfies

$$-m_0(x)\omega^2 u_0(x,\omega) - \Delta_h u_0(x,\omega) = f(x,\omega). \qquad (6)$$

The scattered field u_s can, without approximation, be expressed as a summation along the boundary ∂C, excluding the corner nodes.

$$
\begin{aligned}
u_s(y,\omega) = -\sum_{x \in \partial C} \frac{1}{h^2} \bigg(& u^{\partial C}(x,\omega) G_0^{\partial C_{+1}}(x,y,\omega) \\
& - G_0^{\partial C}(x,y,\omega) u^{\partial C_{+1}}(x,\omega) \bigg), \;\; y \in B \cup \partial C. \quad (7)
\end{aligned}
$$
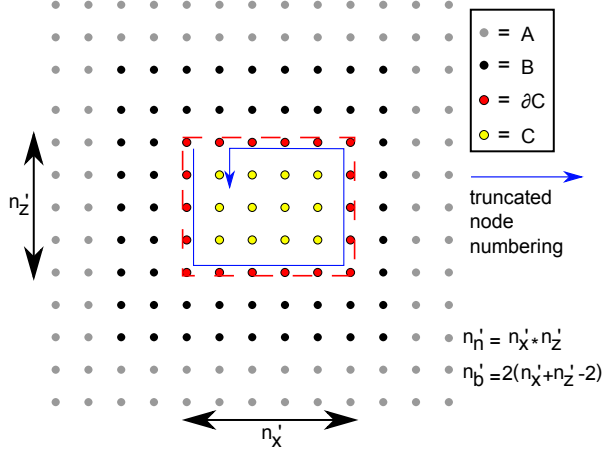
Figure 1: The full mesh Ω is partitioned into A, B, ∂C, and C. The node numbering used in the local solver is spiraling inwards. The number of nodes in the truncated domain is n'_n and the number of boundary nodes is n'_b.

Here we just state the result; a full derivation will be presented in a paper that is currently being prepared for publication. The symbols $u^{\partial C}(x, \omega)$ and $u^{\partial C+1}(x, \omega)$ are the perturbed wavefield on boundary node x and one node to the interior, respectively. The background Green's functions satisfying (6) between the node y, where the scattered field is evaluated, and the node x on the boundary, and one node to the interior are $G_0^{\partial C}(x, y, \omega)$ and $G_0^{\partial C+1}(x, y, \omega)$, respectively.

This equation for the scattered field is used to assemble a system of equations defining the local solver. The unknowns are grouped in vectors such as $\mathbf{u_s}^{\partial C}$ representing the scattered field on ∂C. Similarly, $\mathbf{u}^{\partial C}$ and $\mathbf{u}^{\partial C+i}$ represent the wavefield in the perturbed model m on ∂C and i layers to the interior, respectively. The node numbering in the truncated domain follows the spiraling pattern illustrated in Figure 1.

$$
\begin{pmatrix}
-\mathbf{I} & \mathbf{I} & & 0 \\
\hline
\mathbf{I} & \mathbf{G}^{\partial C+1} & -\mathbf{G}^{\partial C} & \\
\hline
\mathbf{0} & & -\mathbf{m}(x)\omega^2 & -\Delta_h
\end{pmatrix}
\begin{pmatrix}
\mathbf{u_s}^{\partial C} \\
\mathbf{u}^{\partial C} \\
\mathbf{u}^{\partial C+1} \\
\mathbf{u}^{\partial C+2} \\
\vdots
\end{pmatrix}
=
\begin{pmatrix}
\mathbf{u_0}^{\partial C} \\
0 \\
0 \\
0 \\
\vdots
\end{pmatrix},
$$

(8)

The matrix in (8) is composed of block matrices. The block $\mathbf{I}$ is the identity matrix of appropriate size. The blocks $\mathbf{G}^{\partial C}$ and $\mathbf{G}^{\partial C+1}$ contain the background Green's functions, from boundary ∂C and one layer to the interior, respectively, to the node y in boundary ∂C where the scattered field is evaluated. The block $\mathbf{G}^{\partial C+1}$ contains the functions $G_0^{\partial C+1}(x, y, \omega)$ from equation 7 and the block $\mathbf{G}^{\partial C}$ contains the functions $G_0^{\partial C}(x, y, \omega)$, where y is now a boundary node. These Green's function block matrices are the only dense blocks. Equation 8 is compartmentalized into three rows by horizontal lines. The first block row represents (4) on all boundary nodes in ∂C. The second block row expresses the scattered wavefield in terms of the perturbed wavefield through (7) for each boundary node. The third block row is the second-order-accurate Helmholtz operator in the in-

terior of the truncated domain.

PROPERTIES OF THE LOCAL SOLVER

In this section, we first discuss the precomputations required to initialize the local solver defined in (8). After that, we discuss the additional required steps for using the local solver in an inversion context.

Initializing the local solver

In order to compute the local wavefield for a shot there are three sets of Green's functions in (8) that need to be precomputed.

- To fill the block $\mathbf{G}^{\partial C}$, we require the background Green's functions from each of the n'_b boundary nodes to all of the other boundary nodes, with n'_b defined in Figure 1.

- The block $\mathbf{G}^{\partial C+1}$ requires precomputation of the background Green's functions from each node on the boundary to all nodes one layer to the interior of ∂C.

- The background wavefield on boundary ∂C is defined as $\mathbf{u_0}^{\partial C}$. It requires the background Green's functions from each source location to all the n'_b boundary nodes.

With these background Green's functions, the exact local wavefield is computed in the truncated domain by solving (8). It includes all interactions between perturbations in the interior of the truncated domain (i.e., domain C) and any inhomogeneity outside of the truncated domain. All orders of scattering are computed exactly, and the solution of (8) for each shot is, up to machine precision, the same as what the full domain Helmholtz solver would have produced for any perturbation satisfying (3).

Using the local solver in an inversion context

To exclusively use the local solver in an inversion, we need to be able to evaluate the objective function corresponding to the locally perturbed model. When the solution of (8) is available, we can use that to compute the scattered field at the receiver locations y through (7). The wavefield u in the perturbed model is evaluated at the receiver locations by adding the background wavefield u_0 from the source to this scattered wavefield u_s. This requires additional background Green's functions from the receiver locations to the nodes in ∂C and one layer to the interior as well as to the source locations.

With all these precomputed background Green's functions, we are able to compute the perturbed wavefield in the truncated domain $\partial C \cup C$ and evaluate the residuals at the receivers using the local solver. In the computation of the adjoint field, the residuals act as source terms at the receiver locations. Since we have the background Green's functions from the receiver locations to the truncated domain, we can compute the adjoint wavefield resulting from these residual forces locally. Each residual source corresponds to a right-hand side vector in (8). Instead of computing the adjoint wavefield contribution of each source individually and summing the solutions, because of linearity, we can sum the right hand side terms prior to solving

Toward target-oriented FWI: An exact local wave solver applied to salt boundary inversion

(8). This way, the local solver computes the adjoint wavefield from the residuals of a shot using a single solve. After the required Green's functions are computed using a full domain solver, we can generate exactly the same forward and adjoint wavefields in the truncated domain using the local solver. Hence, exactly the same FWI gradient is obtained when these wavefields are crosscorrelated as would be obtained when solving in the full domain.

The matrix in (8) is of size $n_b' + n_n'$ and the number of unknowns is much smaller than the full domain equivalent, which makes the local solves much faster. Instead of using a single truncated domain we can also use multiple disjoint domains. The equivalence of the solutions between the local and full domain solvers remains as long as the model perturbations are restricted to the multiple domains. All orders of scattering between the perturbations in the domains and the inhomogeneous background model are conserved. Derivation and application will be presented in the paper that is currently being prepared.

APPLICATION TO SALT BOUNDARY INVERSION

The accuracy of the salt body in the velocity model plays an important role in determining the quality of the subsalt migrated image. In this paper, we attempt to improve a specific section of the subsalt migrated image by improving the overlying salt body in the velocity model. When using the automatic salt updating code introduced by Lewis et al. (2012), we need the FWI gradient along boundary of the salt to change its shape in the velocity model. Since we only need the gradient at the salt and not in the entire velocity model, this is a good application for the local solver.
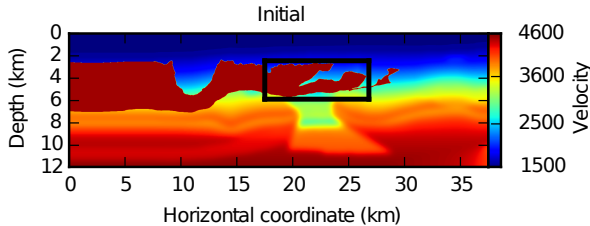

Figure 2: The initial velocity model with the black box representing the truncated domain in which we attempt to improve the salt boundary estimate.

Problem description
We apply the combination of the local solver and the salt updating code on a section of the BP2004 velocity model. We start with the initial velocity model in Figure 2. The initial sediment velocity is obtained by smoothing the true sediment velocity. The boundary of the initial salt body is obtained from the true salt body by applying oscillatory perturbations to it with amplitude up to 150 m. The largest deviations are present at the salt bottom, which is to be expected because poor illumination increases the uncertainty. To improve the salt boundary estimate, we use the local solver to generate wavefields within the truncated domain, represented by the black box in Figure 2. The true and the initial model are different inside and out-
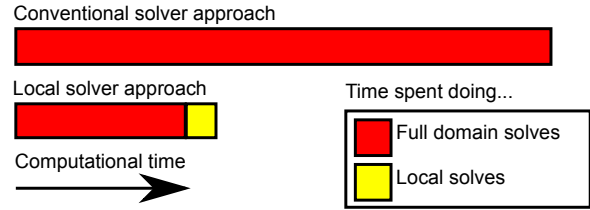

Figure 3: Schematic cost comparison for inversion in the truncated domain using a full versus a local domain solver.

side the black box. In this experiment, we use the same constant density acoustic finite difference code for generating the data and the Green's functions. No noise is added to the data. We simulate a seismic survey with 200 shots, and we use 500 unique receiver locations equally spread over the surface. Each shot includes receiver locations with an offset up to 10 km. We perform a frequency sweep with inversion taking place at the frequencies 2.5, 3.0, 3.5, 4.5, 5.5, and 7.0 Hz.

Cost analysis
At each FWI iteration of each frequency, we first compute the gradient, which requires 200 forward wave solves and 200 adjoint wave solves (i.e., one for each shot). We then perform a line-search requiring on average two evaluations of 200 wave solves each. This brings the total number of wave solves at a specific frequency to 8000 when 10 iterations take place. The computational time if we had used a full domain solver for these 8000 wave solves is represented by the upper bar in Figure 3. For this specific example, the number of background Green's functions that must be precomputed is 2550. The red component of the lower bar represents the cost of precomputing these. The yellow component of the lower bar corresponds to the amount of computational time the local solver needs to compute the same 8000 wavefields locally. A local wave solve is approximately 20 times faster than a full domain solve for this example.

Figure 3 shows that as long as we are willing to accept that model updates are restricted to the truncated domain, using the local solver is an economical choice. An additional advantage of the local solver is that the precomputation of the background Green's functions is the majority of the work and it only needs to be done once. Performing multiple simultaneous local inversions with different inversion parameters is cheap because of this. Graphically, the cost of each additional inversion using the local solver is visualized by adding another yellow block to the bottom horizontal bar in Figure 3. This is far cheaper than performing an additional inversion using the full domain solver, which would correspond to top bar in Figure 3. The local solver also makes the inversion procedure more interactive, because the duration of each inversion is reduced by a factor of 20 in this example.

We again stress that each locally computed wavefield is exactly the same as the solution of the full domain solver as long as we restrict model updates to the interior of the truncated domain. This can be seen in Figure 4. The solutions have a relative difference on the order of $1e-13$, independent of the shape

Toward target-oriented FWI: An exact local wave solver applied to salt boundary inversion
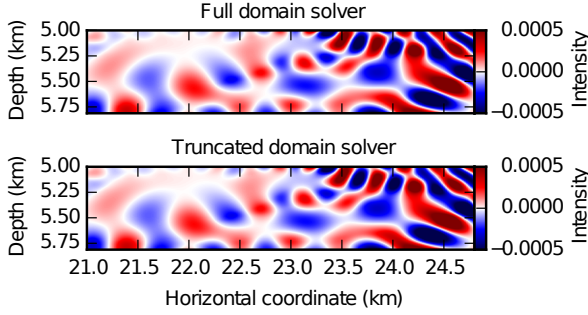

Figure 4: Real part of the wavefield within the truncated domain. The solutions from the full domain solver and the local solver are displayed for a shot at the frequency 2.5 Hz.

and amplitude of the model perturbation. Using $|.|_2$ for the least squares norm, the relative difference is defined as

$$\varepsilon = \frac{|u_f - u_t|_2}{|u_f|_2}. \tag{9}$$

Results

The local solver significantly improves the salt boundary estimate at most locations. Figure 5 shows updates in the order of 150 m. Outside of the truncated domain, the inverted velocity model is equal to the initial velocity model, because updates were limited to the truncated domain. So, the local inversion results in Figure 5 are embedded in the bulk initial model of Figure 2.

We use the true, initial, and inverted velocity models in reverse time migration (RTM) with data synthesized using a variable density time domain solver. Figure 6 compares the migration results in a region just below the right side of the truncated domain. The migration in the initial velocity model is severely distorted by the incorrect shape of the overlying salt. Many
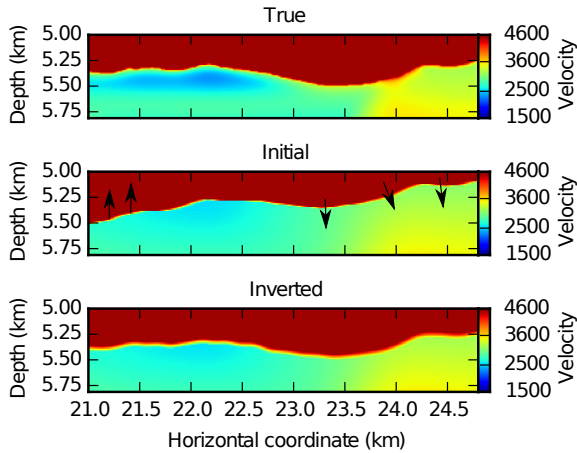

Figure 5: The local inversion significantly improved the salt boundary at most locations. Here we show improvement at a representative section of the salt bottom. The arrows show how the initial model salt boundary was changed.

of the features that are present in the true model have lower amplitude or are not recognizable at all. It is easy to observe how the improved shape estimate of the salt body enhances the migrated images. This is because the inverted salt shape better focuses the energy.
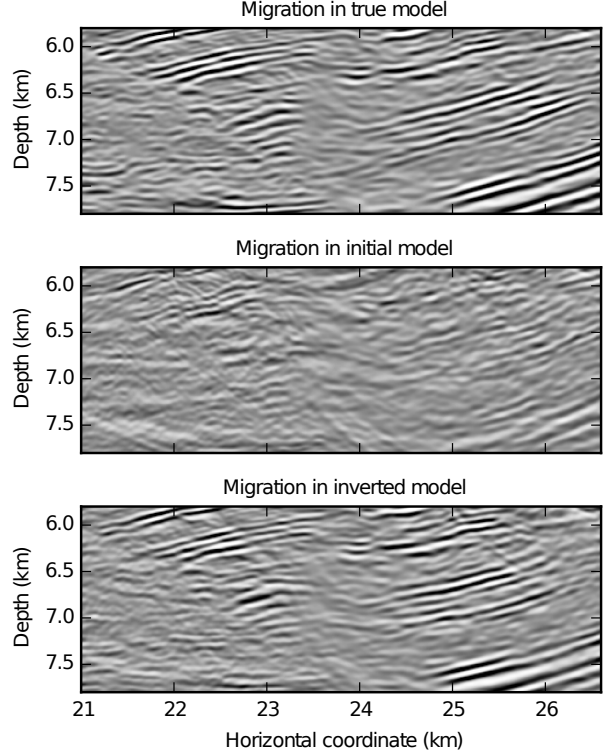

Figure 6: Comparison of subsalt RTM images on the true, initial, and inverted velocity models

CONCLUSIONS

In this paper, we introduced a local wavefield solver. We demonstrated how the local solver generates exactly the same wavefield as a full domain solver, without making any approximation. We then used the local solver to improve the estimate of the salt boundary. When we have specific interest in improving the migrated image below the salt body, improving the shape of the overlying salt body has a large impact. For the purpose of updating the salt boundary locally, computing full domain gradients is wasteful. In this paper, we showed that using the local solver for this inversion is economical. The velocity model is improved with positive results for the subsalt migrated image.

Toward target-oriented FWI: An exact local wave solver applied to salt boundary inversion

REFERENCES

Berryhill, J., 1984, Wave-equation datuming before stack: Geophysics, **49**, no. 11, 2064–2066.

Gillman, A., A. Barnett, and P.-G. Martinsson, 2013, A spectrally accurate direct solution technique for frequency-domain scattering problems with variable media: arXiv preprint arXiv:1308.5998.

Grote, M., and I. Sim, 2011, Local nonreflecting boundary condition for time-dependent multiple scattering: Journal of Computational Physics, **230**, 3135–3154.

Haffinger, P., 2012, Seismic broadband full waveform inversion by shot/receiver refocusing: PhD thesis, TU Delft, Delft, The Netherlands.

Herrmann, F., I. Hanlon, T. van Leeuwen, X. Li, B. Smithyman, and H. Wason, 2013, Frugal full-waveform inversion: From theory to a practical algorithm: The Leading Edge, **32**.

Krebs, J., J. Anderson, D. Hinkley, R. Neelamani, S. Lee, A. Baumstein, and M. Lacasse, 2009, Fast full-wavefield seismic inversion using encoded sources: Geophysics, **74**, WCC177–WCC188.

Lewis, W., B. Starr, and D. Vigh, 2012, A level set approach to salt geometry inversion in full-waveform inversion: SEG Technical Program Expanded Abstracts 2012, 1–5.

Métivier, L., R. Brossier, J. Virieux, and S. Operto, 2013, Full waveform inversion and the truncated newton method: SIAM Journal on Scientific Computing, **35**, B401–B437.

Robertsson, J., and C. Chapman, 2000, An efficient method for calculating finite-difference seismograms after model alterations: Geophysics, **65**, 907–918.

Teng, Z.-H., 2003, Exact boundary condition for time-dependent wave equation based on boundary integral: Journal of Computational Physics, **190**, 398–418.

van Manen, D.-J., J. O. A. Robertsson, and A. Curtis, 2007, Exact wave field simulation for finite-volume scattering problems: The Journal of the Acoustical Society of America, **122**, EL115–EL121.

Wang, S., M. V. de Hoop, and J. Xia, 2011, On 3D modeling of seismic wave propagation via a structured parallel multifrontal direct Helmholtz solver: Geophysical Prospecting, **59**, 857–873.

Wiggins, J., 1984, Kirchhoff integral extrapolation and migration of nonplanar data: Geophysics, **49**, no. 8, 1239–1248.

Zepeda-Núñez, L., and L. Demanet, 2014, The method of polarized traces for the 2D Helmholtz equation: arXiv preprint arXiv:1410.5910.